006 A PRIORI PREDICTION OF RELATIVE PERMEABILITY AND CAPILLARY PRESSURE FROM PORE-SCALE MODELLING

PÅL-ERIC ØREN, STIG BAKKE and OLE JAKOB ARNTZEN
Statoil Research Centre, Postuttak, 7005 Trondheim, Norway

Abstract
We reconstruct 3-D sandstone models that give a realistic description of the complex microstructure observed in actual sandstones. Pore networks replicating the microstructure of the reconstructed samples are constructed and used as input to a two-phase network model. The network model simulates primary drainage and water injection for both water wet and mixed wet systems. Predicted transport properties for different reconstructed sandstones are found to be in good agreement with available experimental data. The agreement provides a strong hint that it is possible to *a priori* predict average transport properties from the associated pore-scale parameters.

Introduction
The microstructure of a porous medium and the physical characteristics of the solid and the fluids that occupy the pore space determine several macroscopic properties of the medium. These properties include transport properties of interest such as permeability, electrical conductivity, relative permeability, and capillary pressure. In principle, it should be possible to determine these properties by appropriately averaging the equations describing the physical processes occurring on the pore-scale. This approach requires a detailed understanding of the displacement processes on the pore-scale and a complete description of the morphology of the pore space. One commonly applied tool in this approach is the network model. Since the pioneering work of Fatt[1-3], network models have been used extensively to study different displacement processes in simple or idealised porous media. The studies by Blunt and coworkers[4-6] and Jerauld and Salter[7] are good examples of the success of this approach. Seldom, however, are network models claimed to be representative of real rocks.

The extension of network modelling techniques to real rocks is hampered by the difficulty of adequately describing the complex nature of the pore space. Techniques such as microtomographic imaging and serial sectioning provide a detailed description of the pore space at micrometer resolution. In practice, however, information about the microstructure of reservoir rocks is limited to 2-D thin section images of the pore space and to the pore throat entry sizes determined from mercury injection data. These data are insufficient to construct directly a 3-D network replica of the microstructure. As a result, most prior applications of network modelling techniques have invoked simplifying assumptions about unmeasured topological and geometrical features of the pore space. This has prevented network models from being used as a predictive tool, thus greatly limiting their application in the oil industry.

In the present work, geostatistical information obtained from image analysis of 2-D thin sections are used to generate a reliable reconstruction of the complex rock-pore system in 3-D. The network representation of the pore space is constructed from topological and geometrical analyses of the fully characterised reconstructed sample. The pore network is subsequently used as input to network simulators of single- and two-phase flow. Predicted transport properties for three different reconstructed sandstones are compared with experimental data.

Sandstone Reconstruction
A sandstone sample and its petrographical parameters are the end result of all the geological and hydrodynamical processes that have affected the sedimentary basin. We do not attempt to model the

detailed dynamics of these very complex processes. Instead, we reconstruct the 3-D sandstone by simulating the results of the main sandstone forming processes - *sedimentation*, *compaction*, and *diagenesis*. Petrographical data obtained from image analysis of 2-D thin sections are used as input[8].

Sedimentation. Sedimentation is modelled by randomly selecting grains from a measured grain-size distribution curve and then deposit them into a pre-defined bound-box. For simplicity, all the detrital grains are modelled as being spherical. The exact location in the bound-box where new grains deposit depends on whether the sedimentation process occurs in a low- or high-energy environment. Sandstones are normally the results of high-energy depositional events. High-energy sedimentation is modelled by placing each new grain at the lowest available position (global minimum) in the bound-box. A detailed description of the sedimentation modelling is given elsewhere[9].

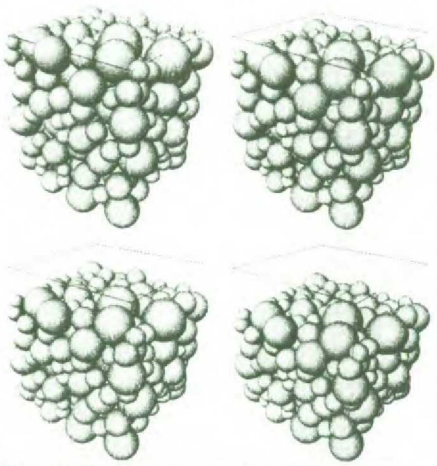

Fig. 1. Compaction modelling for compaction factors = 0.0, 0.1, 0.2, and 0.3.

Compaction. Compaction is an important agent for porosity reduction in sandstones during burial. The reduction in porosity is usually caused by vertical shortening in response to stresses from the overburden. The results of compaction are modelled similarly to that described by Bryant *et al.*[10]. The z-co-ordinate of every sandgrain centre is shifted vertically downwards according to the formula $Z = Z_0(1-\lambda)$ where Z_0 is the original position and Z is the new one. λ is a compaction factor that describes the degree of compaction (**Fig. 1**). Compaction modelling causes grains to interpenetrate. This is analogous to pressure solution at grain contacts. We assume that the interpenetration results in no deformations of the grains. The material corresponding to the grain interpenetration may be dissolved and washed out of the system or it may be re-precipitated as quartz cement.

Diagenesis. Currently, only a simplified subset of known diagenetic processes are modelled: quartz cement overgrowth and subsequent clay coating of the free surface. The overgrowth of quartz cement on the detrital grains is modelled similarly to that described by Schwartz and Kimminau[11]. The quartz cement thickness h_c depends on the rate and on the direction of cement growth according to the formula $h_c = \min(a\Delta^k, \Delta)$ where Δ is the distance between the surface of the grain and the surface of its Voronoi polyhedron[8], a controls the amount of quartz cement growth whilst k determines the rate and direction of growth. The effect of the growth exponent k is illustrated in **Fig. 2**. Positive values of k favour growth towards the pore bodies whilst negative values favour growth towards the throats. If $k = 0$, quartz cement deposits as concentric overgrowth on the detrital grains.

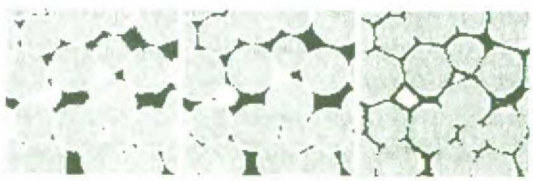

Fig. 2. Cross-sections illustrating the modelling of quartz cement for k = -1 (left), k = 0 (middle) and k = +1 (right). The porosity is constant.

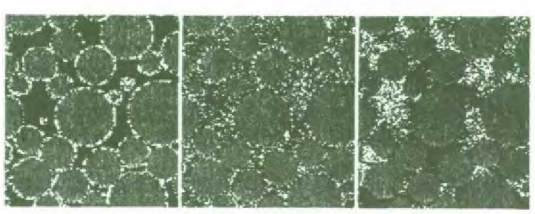

Fig. 3. Cross-sections illustrating the modelling of clay coating. Pore-lining (left), pore-filling (right), and a mixture of the two types (middle).

Different types of authigenic clays may precipitate in the pore space of the sandstone during the diagenetic stages. Authigenic clays clog and sub-divide pore space and generate micro porosity. Pores within the micro porosity are typically one or two orders of magnitude less than the intergranular pores. The permeability of these pores is assumed to be negligible compared to that of the intergranular pore space. The morphology of precipitated clays can be characterised as pore-lining, pore-filling, or pore-bridging. Typical examples include chlorite, kaolinite, and illite, respectively. Pore-lining clays are modelled by randomly precipitating clay voxels on the surfaces of the detrital grains or the quartz cement (**Fig. 3** (left)). Pore-filling clays are modelled using a clay clustering routine that causes new clay voxels to precipitate preferentially in selected pore

bodies (**Fig. 3** (right)). The total amount of clay to be precipitated is extracted from petrographical analysis[8]. Pore-bridging clays are currently not included in the model.

Pore Network

An example of a reconstructed sandstone is shown in **Fig. 4**. Although it is possible to perform flow simulations directly on the chaotic pore space of the sandstone model, it can only be done at considerable computational expense. It is therefore necessary to construct a pore network that replicates the essential features of the microstructure that are relevant to fluid flow.

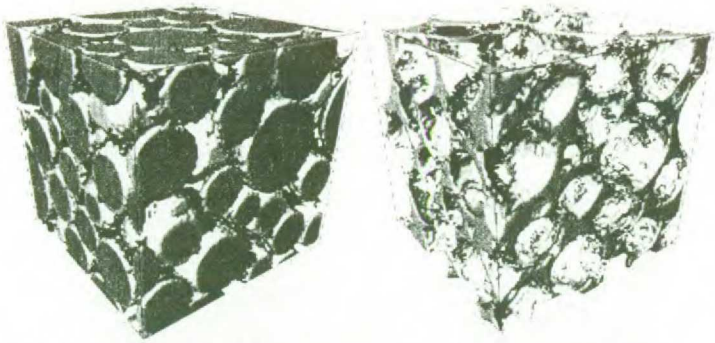

Fig. 4. A small cube of a reconstructed sandstone (left) and its complementary pore space (right). The linear scale of the model is 100 voxels (0.75mm) on each side.

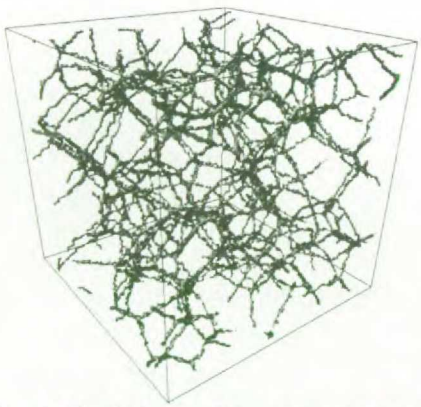

Fig. 5. The skeleton of the reconstructed pore space shown in Fig. 4.

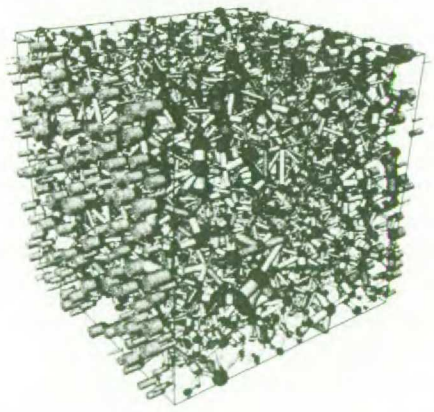

Fig. 6. Ball-and-stick illustration of a generated pore network. The network contains 3305 nodes and 8336 links.

Topology. The topology of the pore network is determined by constructing the skeleton or the "node-and-link" graph of the pore space. The construction of the skeleton is done most naturally in terms of the Voronoi polyhedra of the grains. The skeleton corresponds to the vertices and edges of these polyhedra. It is defined by the points that have neighbour voxels from three or more different ultimately dilated grains. The vertices of the polyhedra have neighbour voxels from four or more different ultimately dilated grains and correspond to the nodes in the pore network. An example of a skeleton constructed by this procedure is depicted in **Fig. 5**. The skeleton provides information about the location of network nodes (approximate pore body centres), the spacing between the nodes, and about the connectivity of each node (co-ordination number).

Geometrical Characterisation. The detailed geometry of the pore space is highly chaotic. To retain a tractable problem, it is necessary to characterise it by a few intrinsic parameters that retain the essential features relevant to fluid flow. The skeleton is a natural starting point for the geometrical characterisation. For each skeleton voxel, the pore space between adjoining nodes is mapped in a plane normal to its local direction using a rotating vector[9]. The inscribed radius corresponding to the minimum constriction is recorded and used as a measure of the pore throat size. Pore body sizes are determined similarly. The size of a pore body is defined by the radius of the largest sphere that can be locally inscribed from the geometrical centre point of the pore body (*i.e.*, the skeleton node).

A key characteristic of porous media is the angular corners of pores. Angular corners retain wetting fluid and allow two or more fluids to flow simultaneously through the same pore. In the present work, the shape of every pore body and throat is described in terms of a dimensionless shape factor G which is defined as[12] $G = A/P^2$ where A is the average cross-sectional area of the pore body or throat and P is the corresponding perimeter length. The area and perimeter length are determined using standard image analysis techniques. The shape factor replaces the irregular shape of a pore body or throat by an equivalent irregular triangular shape. The shape factor ranges

from zero for a slit shaped pore to 0.048 for an equilateral triangular pore. Further details of the geometrical characterisation are given elsewhere[8,9].

Results

A ball-and-stick illustration of a generated pore network is shown in **Fig. 6**. Single and two-phase flow in the network are simulated using a network model that has been described before[8,9,13]. The network model simulates drainage and water injection for both water wet and mixed wet systems. We use the network model to predict transport properties for three different reconstructed sandstones. The data from the simulations are then compared with available experimental data.

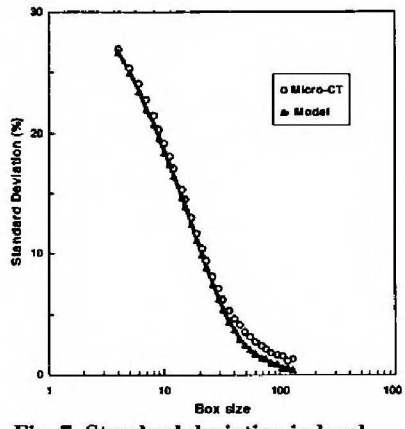

Fig. 7. Standard deviation in local porosity for the model and actual sample of Fontainebleau sandstone.

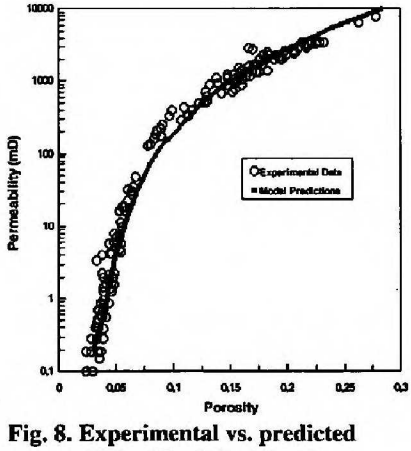

Fig. 8. Experimental vs. predicted permeability (Fontainebleau).

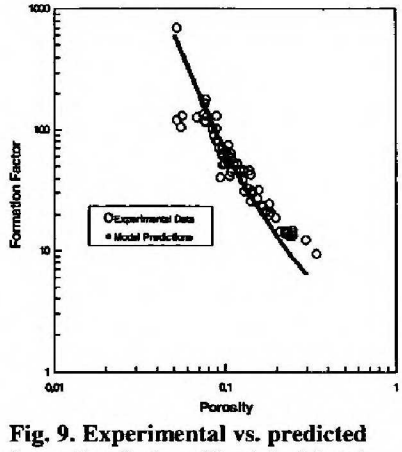

Fig. 9. Experimental vs. predicted formation factors (Fontainebleau).

Fontainebleau Sandstone. The Fontainebleau sandstone is an aeolan fine grained quartzite. Thin section analyses reveal that it is well sorted with an average grain size of around 200μm. A model of Fontainebleau sandstone was reconstructed from thin section data and then compared with microtomographic images of the actual sample. **Fig. 7** compares the standard deviation in local porosity for the two samples. Local porosity distributions were measured using a moving box technique with a logarithmic increase in box size. This ensures that both local and global variations in porosity are captured. The model closely mimics the actual sample, except at large box sizes where the variation in porosity is too small. This suggests that the reconstructed model does not capture all the global heterogeneities that are present in the real sample.

The porosity and permeability of Fontainebleau sandstone samples vary widely. The variation in these properties is due almost entirely to the degree of quartz cementation. Using the reconstructed model as basis, we generated models with different porosity by varying the amount of quartz cement. The predicted permeability versus porosity trend is compared with published data[14] in **Fig 8.** Although the measured permeabilities span nearly five orders of magnitude, the predicted permeability versus porosity trend is in good agreement with the experimental one. **Fig 9** compares predicted and measured[15,16] formation factors. Except for some deviations at high porosities, the predicted formation factors are in good agreement with the measured ones. The close match between predicted and measured data demonstrates that our sandstone model successfully simulates the results of real diagentic processes and adequately predicts the behaviour for single phase flow.

Bentheimer Sandstone. This well-sorted sandstone is composed mainly of quartz (70-80%), feldspar (20-25%), and authigenic clays (2-3%). The main clay component is pore-filling kaolinite. Thin section images of three twin samples were analysed and used to reconstruct six realisations of a water wet Bentheimer sandstone. The calculated permeability for the reconstructed sample was 3010mD whilst the experimentally measured one was 2160mD. The predicted formation factor was 11.7 which is in excellent agreement with the measured value of 12.0. **Fig. 10** compares computed and experimentally measured (porous plate method) drainage capillary pressures. The calculated capillary pressure curve is in good agreement with the measured one and we correctly predict the threshold displacement pressure and the connate water saturation.

Predicted and measured (steady state) relative permeabilities for primary drainage and waterflooding are compared in **Figs. 11** and **12**, respectively. The network simulator clearly reproduces the experimental characteristics of the measured data and correctly predicts the waterflood residual oil saturation. At low water saturations, the predicted water permeability is larger than the measured one. This suggest that we overestimate the water conductance in the corners and crevices of oil invaded pore bodies and throats[8].

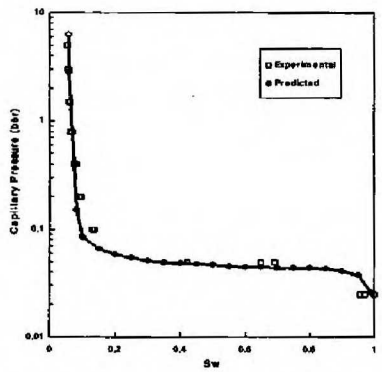

Fig. 10. Experimental vs. predicted capillary pressure (Bentheimer).

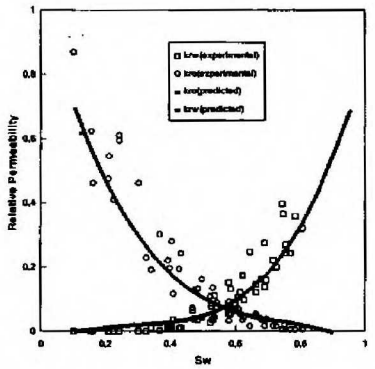

Fig. 11. Experimental vs. predicted drainage relative permeabilities.

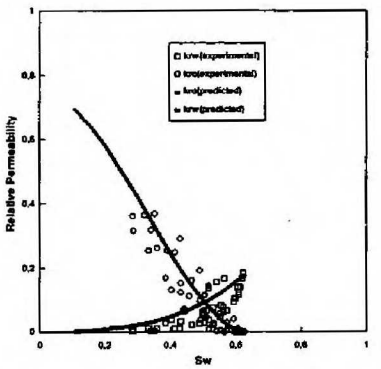

Fig. 12. Experimental vs. predicted waterflood relative permeabilities.

Reservoir Rock. This North Sea Lower Brent reservoir rock is a micacious (10-12 wt%) feltspatic (15-19 wt%) sandstone with abundant pore-filling kaolinite. Thin section images of the rock were analysed and used to reconstruct a 3-D model of the sandstone. The predicted permeability of the model was 420mD whilst the measured permeability was 340mD. The reservoir rock displays a mixed wettability with an Amott wettability index equal to 0.12. Unfortunately, it is not possible to *a priori* assign wettability on the pore-scale. Instead, we investigate how relative permeabilities and waterflood residual oil saturation S_{or} depend on the fraction f of oil invaded pore bodies and throats that become mixed wet[8].

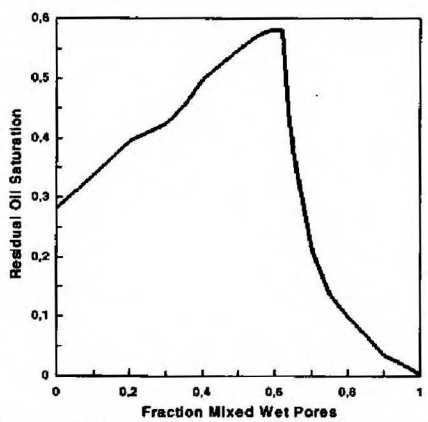

Fig. 13. Waterflood residual oil saturation as a function of the fraction pore bodies and throats that become mixed wet.

Fig. 13 shows how S_{or} depends on the fraction mixed wet pore bodies and throats. For small f, the mixed wet regions of the pore space do not form a continuos cluster. Oil in these regions are thus trapped by water after spontaneous imbibition and S_{or} increases almost linearly with f. Forced water injection (*i.e.*, negative capillary pressures) in this regime results in very little additional oil recovery. At a critical f (around 0.62), mixed wet pore bodies and throats first form a continuous flow path to the outlet. Forced water injection can then displace oil from the mixed wet regions of the pore space and S_{or} drops sharply.

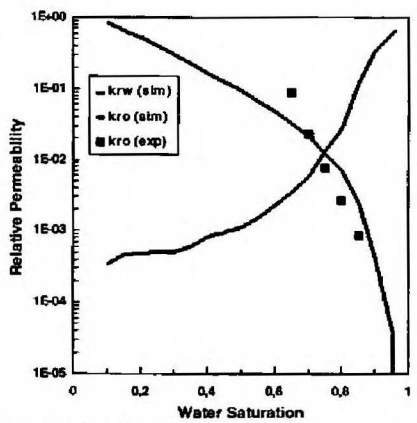

Fig. 14. Predicted oil and water relative permeabilities for the reservoir rock when f = 0.85.

The experimentally determined S_{or} for the reservoir rock is 5%. From **Fig. 13**, this corresponds to f = 0.85. Predicted oil and water relative permeabilities for this case are shown in **Fig. 14**. The experimental data depicted in **Fig. 14** were determined from a single speed centrifuge test using Hagoort's analytical method[17] to compute oil relative permeability. The agreement between the predicted and measured oil relative permeabilities is encouraging. Both the experiments and the simulations show that continuos oil films that exist in mixed wet pores allow low oil saturations to be reached during forced water injection. The relative permeability to oil, however, is very low.

Conclusions

1. Petrographical data obtained from thin section analysis are used to reconstruct model sandstones that give a realistic description of the complex microstructure exhibited in real sandstones.
2. Predicted permeabilities and formation factors for a reconstructed Fontainebleau sandstone model correspond well with published data over a wide range of porosity.
3. Predicted drainage and waterflood relative permeability curves for a water wet Bentheimer sandstone are in good agreement with experimental data.
4. Computed waterflood residual oil saturation and oil relative permeabilities for a mixed wet reservoir rock are in fair agreement with experimental measurements.

Acknowledgements

The authors would like to acknowledge Den norske stats oljeselskap a.s. (Statoil) for granting permission to publish this paper. We are indebted to Svein H. Midtlyng for performing the experimental work. We also graciously thank David Stern, Exxon Research Production Company, for providing us with the microtomography data.

References

1. Fatt, I.: "The Network Model of Porous Media I. Capillary Pressure Characteristics," *Trans. AIME* (1956), **207**, 144.
2. Fatt, I.: "The Network Model of Porous Media II. Dynamic Properties of a Single Size Tube Network," *Trans. AIME*, (1956), **207**, 160.
3. Fatt, I.: "The Network Model of Porous Media III. Dynamic Properties of Networks with Tube Radius Distribution," *Trans. AIME*, (1956), **207**, 164.
4. Blunt, M.J. and King, P.R.: "Relative Permeabilities from Two- and Three-Dimensional Pore-Scale Network Modelling", *Transport in Porous Media*, (1991), **6**, 407.
5. Blunt, M.J., King, M., and Scher, H.: "Simulation and Theory of Two-Phase Flow in Porous Media", *Phys. Rev. A*, (1992), **46**, 7680.
6. Blunt, M.J.: "Pore Level Modelling of the Effects of Wettability", submitted to *SPEJ*, (1997).
7. Jerauld, G.R. and Salter, S.J.: "The Effect of Pore-Structure on Hysteresis in Relative Permeability and Capillary Pressure: Pore-Level Modelling", *Transport in Porous Media*, (1990), **5**, 103.
8. Øren, P.E., Bakke, S., and Arntzen, O.J.: "Extending Predictive Capabilities to Network Models", SPE 38880, presented at the 1997 SPE Annual Technical Conference and Exhibition, Oct. 5-8.
9. Bakke, S. and Øren, P.E.: "3-D Pore-Scale Modelling of Sandstones and Flow Simulations in the Pore Networks", *SPEJ*, (1997), **2**.
10. Bryant, S., Cade, C., and Mellor, D.: "Permeability Prediction From Geological Models", *AAPG Bulletin*, (1993), **77**, 1338.
11. Schwartz, L.M. and Kimminau, S.: "Analysis of Electrical Conduction in the Grain Consolidation Model", *Geophysics*, (1987), **52**, 1402.
12. Mason, G. and Morrow, N.R.: "Capillary Behaviour of a Perfectly Wetting Liquid in Irregular Triangular Tubes," *J. of Colloid and Interface Science*, (1991), **141**, 262.
13. Øren, P.E., Bakke, S., Nilsen, L.S., and Henriquez, A.: "Prediction of Relative Permeability and Capillary Pressure from Pore-Scale Modelling", proceedings of the 1996 European Conference on the Mathematics of Oil Recovery, Leoben, Austria, Sept. 3-6.
14. Bourbie, T. and Zinszner, B.: "Hydraulic and Acoustic Properties as a Function of Porosity in Fontainebleau Sandstone", *J. of Geophysical Research*, (1985), **90**, 11524.
15. Jacquin, C.G.: " Correlation entre la Permeabilite et les Caracteristiques Geometriques du gres de Fontainebleau", *Rev. Inst. Fr. Pet.*, (1964), **19**, 921.
16. Fredrichs, J.T., Greaves, K.H., and Martin, J.W.: "Pore Geometry and Transport Properties of Fontainebleau Sandstone", *Int. J. Rock Mech. Min. Sci. & Geomech.*, (1993), **30**, 691.
17. Hagoort, J.: "Oil Recovery by Gravity Drainage", *SPEJ*, (1980), **20**, 139.